

Comparative quantitative assessment of the human corneal sub-basal nerve plexus by *in vivo* confocal microscopy and histological staining

BS Kowtharapu^{1,2,8}, K Winter^{3,4,8}, C Marfurt⁵,
S Allgeier⁶, B Köhler⁶, M Hovakimyan¹,
T Stahnke¹, A Wree⁷, O Stachs¹ and
RF Guthoff^{1,2}

Abstract

Purpose This study was designed to compare and contrast quantitative data of the human corneal sub-basal nerve plexus (SBP) evaluated by two different methods: *in vivo* confocal microscopy (IVCM), and immunohistochemical staining of *ex vivo* donor corneas.

Methods Seven parameters of the SBP in large-scale IVCM mosaicking images from healthy subjects were compared with the identical parameters in *ex vivo* donor corneas stained by β -III-tubulin immunohistochemistry. Corneal nerve fiber length (CNFL), corneal nerve fiber density (CNFD), corneal nerve branch density (CNBD), average weighted corneal nerve fiber tortuosity (CNFTo), corneal nerve connection points (CNCP), average corneal nerve single-fiber length (CNSFL), and average weighted corneal nerve fiber thickness (CNFTh) were calculated using a dedicated, published algorithm and compared.

Results Our experiments showed significantly higher values for CNFL (50.2 vs 21.4 mm/mm²), CNFD (1358.8 vs 277.3 nerve fibers/mm²), CNBD (847.6 vs 163.5 branches/mm²), CNFTo (0.095 vs 0.081 μm^{-1}), and CNCP (49.4 vs 21.6 connections/mm²) in histologically staining specimens compared with IVCM images. In contrast, CNSFL values were higher in IVCM images than in histological specimens (32.1 vs 74.1 μm). No significant difference was observed in CNFTh (2.22 vs 2.20 μm) between the two groups.

Conclusions The results of this study have shown that IVCM has an inherently lower

resolution compared with *ex vivo* immunohistochemical staining of the corneal SBP and that this limitation leads to a systematic underestimation of several SBP parameters. Despite this shortcoming, IVCM is a vital clinical tool for *in vivo* characterization, quantitative clinical imaging, and evaluation of the human corneal SBP.

Eye (2017) 31, 481–490; doi:10.1038/eye.2016.220; published online 4 November 2016

Introduction

In vivo confocal microscopy (IVCM) of the cornea offers unique opportunities for non-invasive visualization of corneal nerves *in vivo* and observation of changes that occur in the sub-basal nerve plexus (SBP) during health and disease. Alterations of SBP morphological parameters derived from IVCM images serve as potential biomarkers for early diagnosis of various neurodegenerative diseases.^{1–4}

However, the ability of IVCM to adequately resolve intimate details of SBP anatomy remains incompletely understood since the field of view of a conventional IVCM image is relatively small (400 × 400 μm^2) and might be insufficient for reliable assessment of SBP morphology.⁵ Advancements in imaging extended areas of the corneal SBP by creating large-scale montages^{6–8} have substantially alleviated this principal limitation of IVCM.

Accurate quantification of SBP morphological parameters remains another important concern that must be solved before the usage of IVCM can be translated into clinical practice. Several

¹Department of Ophthalmology, University of Rostock, Rostock, Germany

²Institute for Biomedical Engineering, University of Rostock, Rostock, Germany

³Institute of Anatomy, Faculty of Medicine, University of Leipzig, Leipzig, Germany

⁴Institute for Medical Informatics, Statistics and Epidemiology (IMISE), University of Leipzig, Leipzig, Germany

⁵Indiana University School of Medicine-Northwest, Gary, IN, USA

⁶Institute for Applied Computer Science, Karlsruhe Institute of Technology, Karlsruhe, Germany

⁷Institute of Anatomy, Rostock University Medical Center, Rostock, Germany

Correspondence: RF Guthoff, Department of Ophthalmology, University of Rostock, Doberanerstr. 140, Rostock 18057, Germany
Tel: +49 381 494 8545;
Fax: +49 381 494 8502.
E-mail: rudolf.guthoff@uni-rostock.de

⁸These authors contributed equally to this work.

Received: 15 April 2016
Accepted in revised form: 9 September 2016
Published online: 4 November 2016

rapid image-processing methods for the morphological quantification of corneal cellular structures in IVCM images^{9–13} have been developed and applied to the quantification of SBP in various disease conditions. During the image quantification process, a major point to be considered is intrinsic inhomogeneity of the SBP nerve fiber network pattern which can lead to significant differences among images in various calculated parameters.⁵

Immunohistochemistry (IHC) allows studying the anatomical pattern of specific cellular constituents in histological sections and thereby serves as an essential connecting link between basic science and clinical medicine.^{14–16} IHC has been widely used in the field of ophthalmology to obtain comprehensive anatomical descriptions of human corneal nerve innervation patterns and architecture.^{17–19}

While recent advances in imaging by IVCM provide the opportunity to observe corneal nerves in extended areas ranging up to 18 mm²,⁸ immunohistochemical staining of corneal whole mounts, by using an anti-neuronal class III β -tubulin primary antibody, offers visualization of the corneal nerve architecture from the entire central cornea (~6 mm in diameter). A recent study demonstrates that the average sub-basal nerve densities of standard *in vivo* confocal microscopic images are comparable to wide-field mapped composite images.²⁰ Similarly, since the quantification of the SBP morphological parameters was performed entirely after image post processing, images taken from IVCM can be matched with the images of SBP taken from *ex vivo* histological sections to compare and better understand the ability of IVCM to resolve intimate SBP anatomical details. This comparative study of the data from different subjects allows comparison between histology, the gold standard in terms of anatomical structures, and the IVCM information that is used routinely in clinical settings to image the human corneal SBP. Such a comparison study, even though not from the same subjects, can expand our present qualitative knowledge of SBP and would also be necessary to further prove and validate the practicality of using of this imaging device in clinical practice.

Previously, we have demonstrated that the values of the SBP parameters strongly depend on the acquired section's position within the SBP.⁵ Since IVCM studies consistently underestimate the overall density of the corneal innervation due to its lower resolution compared with IHC, the present study is designed to compare data of SBP parameter local variability, in the context of nerve fiber visibility, from IVCM with *ex vivo* anatomic data of histologically stained corneas (two different imaging modalities) to validate the differences in parameters related to SBP quantification in healthy human subjects.

Materials and methods

The present study was conducted on four large-scale SBP images (image area = 2.425 ± 0.004 mm²) of healthy human subjects generated using a IVCM mosaicking technique described earlier²¹ and four large-scale histologically stained regions of healthy human corneal whole mounts (image area = 2.576 ± 0.263 mm²) prepared by the β -III neurotubulin immunohistochemical staining method. The study protocol was approved by the ethics committee of the University Medical Center, Rostock.

Image data acquisition

For the IVCM portion of this study, four healthy subjects from the Rostock University eye clinic were examined after obtaining their written informed consent following the tenets of the Declaration of Helsinki. In all subjects, the central cornea was imaged by IVCM using a Heidelberg Retina Tomograph II (HRT) equipped with the Rostock Cornea Module (RCM) (Heidelberg Engineering GmbH, Heidelberg, Germany) and a water immersion objective (636/0.95 W, 670 nm; Zeiss, Jena, Germany) as previously described.⁹ During the imaging process, the distance from the subject cornea to the microscope lens was kept constant by using a sterile, disposable contact element (TomoCap, Heidelberg Engineering GmbH). Contact between the subject's cornea and the cap was facilitated by applying a thin lubricant layer of Vidisic gel (Bausch & Lomb/Dr Mann Pharma, Berlin, Germany; refractive index 1.35). The examined right eyes were anesthetized by instilling Proparacain 0.5% eye drops (Ursapharm, Saarbrücken, Germany).

The IVCM images were recorded using a dedicated volume scan mode of the HRT.²¹ For each image stack, an SBP image was composed as described in detail elsewhere.²² For each subject, all reconstructed SBP images with common overlapping areas were then combined into a mosaic image with an expanded field of view using a three-step rigid registration approach.²¹

Immunohistochemistry

Immunohistochemical staining of human corneal nerves was performed on corneal sections as described previously.¹⁷ Human corneal buttons were collected from freshly enucleated eyes of healthy donors after obtaining written informed consent from the patients following the tenets of the Declaration of Helsinki. The donor eyes used in this present study did not have any documented past history of ocular problems and none of the donors had a prior history of diabetes or any neurological problems. All of the donor corneas were certified by the eye banks as

suitable for corneal transplantation based on physical inspection and medical records. The central corneal buttons were removed from the donor eyes with a 6.0 mm corneal trephine and placed directly into room temperature 10% (RT) neutral buffered formalin. Death-to-preservation times ranged from 4.5 to 18 h. Tangential sections were prepared at -20°C in a cryostat. The specimen was placed epithelial side facing down on a glass slide and pressed on a flat platform of frozen optimal cutting temperature (OCT) compound on a cryostat. Four $100\text{-}\mu\text{m}$ -thick sections were then cut from the posterior surface of each central corneal button and collected in ice-cold 0.1 M phosphate-buffered saline (PBS). The remaining corneal section in its frozen OCT matrix was then immersed in a petri dish filled with ice-cold PBS to collect 'anterior-cornea whole mounts' (consisting of the entire corneal epithelium along with $\sim 50\text{--}100\ \mu\text{m}$ of anterior stroma) that were released intact into the PBS after melting of the OCT compound.

Before IHC staining, the anterior-cornea whole mounts were incubated in 0.01% hyaluronidase (type IV-S, Sigma-Aldrich) and 0.1% EDTA (Sigma, Munich, Germany) in 0.1 M PBS pH 5.3 overnight at 37°C to increase their permeability. Later, the tissues were rinsed three times for 15 min each in PBS containing 0.3% Triton X-100 (PBS-TX), and incubated for 2 h in blocking serum (1% bovine serum albumin in PBS-TX). The tissues were then incubated overnight at room temperature (RT) in a mouse monoclonal antibody directed against neuronal class III β -tubulin (Tuj1, 1 : 500, Covance, Münster, Germany). After three more PBS-TX rinses, the tissues were incubated for 2 h at RT in secondary antibody (biotinylated horse anti-mouse IgG, 1 : 200; Vector Laboratories, Eching, Germany), rinsed again in PBS-TX, and incubated for 2 h at RT in avidin-biotin-horseradish peroxidase complex (ABC reagent; Vector Laboratories). After three more PBS-TX rinses, the tissues were incubated for 8 min at RT in 0.1% diaminobenzidine (Sigma) and 0.009% H_2O_2 and then rinsed three times in PBS and twice in distilled water. The tissues were then mounted on glass slides, air-dried, dehydrated in graded alcohols, cleared in xylene, and coverslipped with Permount (Fisher Scientific, Wiesbaden, Germany) under weighted coverslips. Digital images were captured by using a slide scanning system (3D Histech Panoramic Scan 150, 3dhistech Kft., Budapest, Hungary) with a $\times 20$ objective. Captured images were rescaled to match pixel sizes of the IVCN images.

Image segmentation and analysis

IVCN and IHC images underwent a series of image-processing steps including enhancement of image contrast and corneal fiber structures, nerve fiber segmentation,

removal of image artifacts, and reconstruction of interrupted nerve fiber progressions in order to obtain optimized SBP networks.³

On the basis of characteristic morphological and topological quantities an analysis of segmented images was performed. The reconnected segmented nerve fiber networks were projected onto the original image areas and all nerve fibers were skeletonized. Subsequently, undirected graphs of all resulting medial lines were generated and special types of skeleton pixels—branching points, end points, and connection points—were identified. Branching points are skeleton pixels with typically three (or less frequently, four) neighboring skeleton pixels indicating the centers of nerve fiber branches. End points are skeleton pixels with only one neighboring skeleton pixel showing the end of a nerve fiber. Connection points are special end points that are located in the immediate vicinity of the image border, suggesting continuation of the fibers beyond the imaged area and thus reflecting topological embedding within the surrounding network. In the present study, a single nerve fiber is defined as a fiber segment terminated by branching points, end points, and/or connection points.

The following SBP parameters were determined: corneal nerve fiber length (CNFL), defined as the total length of all nerve fibers per unit area (mm/mm^2); corneal nerve fiber density (CNFD), defined as the number of nerve fibers per mm^2 ; corneal nerve branch density (CNBD), defined as the number of branching points per mm^2 ; average weighted corneal nerve fiber tortuosity (CNFTo), reflecting variability of nerve fiber directions and defined as absolute nerve fiber curvature/nerve fiber length in (per μm); corneal nerve connection points (CNCP), defined as the number of nerve fibers crossing the area boundary (connections/ mm^2); average corneal nerve single-fiber length (CNSFL), defined as the average length of nerve fibers (μm); and average weighted corneal nerve fiber thickness (CNFTh), measured as mean thickness perpendicular to the nerve fiber course (μm).

Initially, all parameters were calculated for the whole reconstructed image areas to obtain respective reference values. To investigate the potential parameter variance experienced in single image frames (size of a conventional $400 \times 400\ \mu\text{m}$ IVCN image), all possible image frame locations inside the reconstructed areas were identified. A square (384×384 pixels, dimensions of a conventional IVCN image) was slid across the entire images to simulate an examination at every position of the image area, where a hypothetical single IVCN image could be obtained. Values for all SBP parameters were calculated for all the identified possible image frame locations, and collected in an extensive table, together with the coordinates of the frame center. Image preprocessing and

analysis was carried out using Mathematica 9.0.1 (Wolfram Research Inc., Champaign, IL, USA).

Statistical analysis

Visualization was performed using Mathematica 9.0.1 (Wolfram Research Inc.). Visual representation of the local variability of respective SBP parameters was attained by generation of heat maps as described earlier.⁵ For this purpose, after defining the minimum and maximum values, overlays to the original grayscale images were generated. Minimum value color scale was set to red, whereas the maximum value was set to yellow. The remaining values within this range were then color-coded by interpolation to create a combined image that allows quick and distinctive visual comparison between SBP network configuration and ranking of the local parameter value. As a result, regions with high local values appear in yellow and the regions with low local values appear in red. Distribution plots

were generated to illustrate distribution of the respective SBP parameter values. The mean values of all single frames were calculated and added to the respective parameter density plot as a green marker. A dashed red line indicating the respective parameter value of the reference image was also added to these plots.

Statistical analysis was performed with IBM SPSS Statistics (version 22; IBM Corp.; Armonk, New York, NY, USA). Data was tested for normal distribution using the Shapiro–Wilk test. Group comparisons were performed using Mann–Whitney-*U* test. Significance was set at $P < 0.05$. Data were expressed as mean (\pm SD) or median (interquartile range (IQR)) for normally and not normally distributed data, respectively.

Results

Four images each from IVCM and histologically processed corneas were quantified. The representative

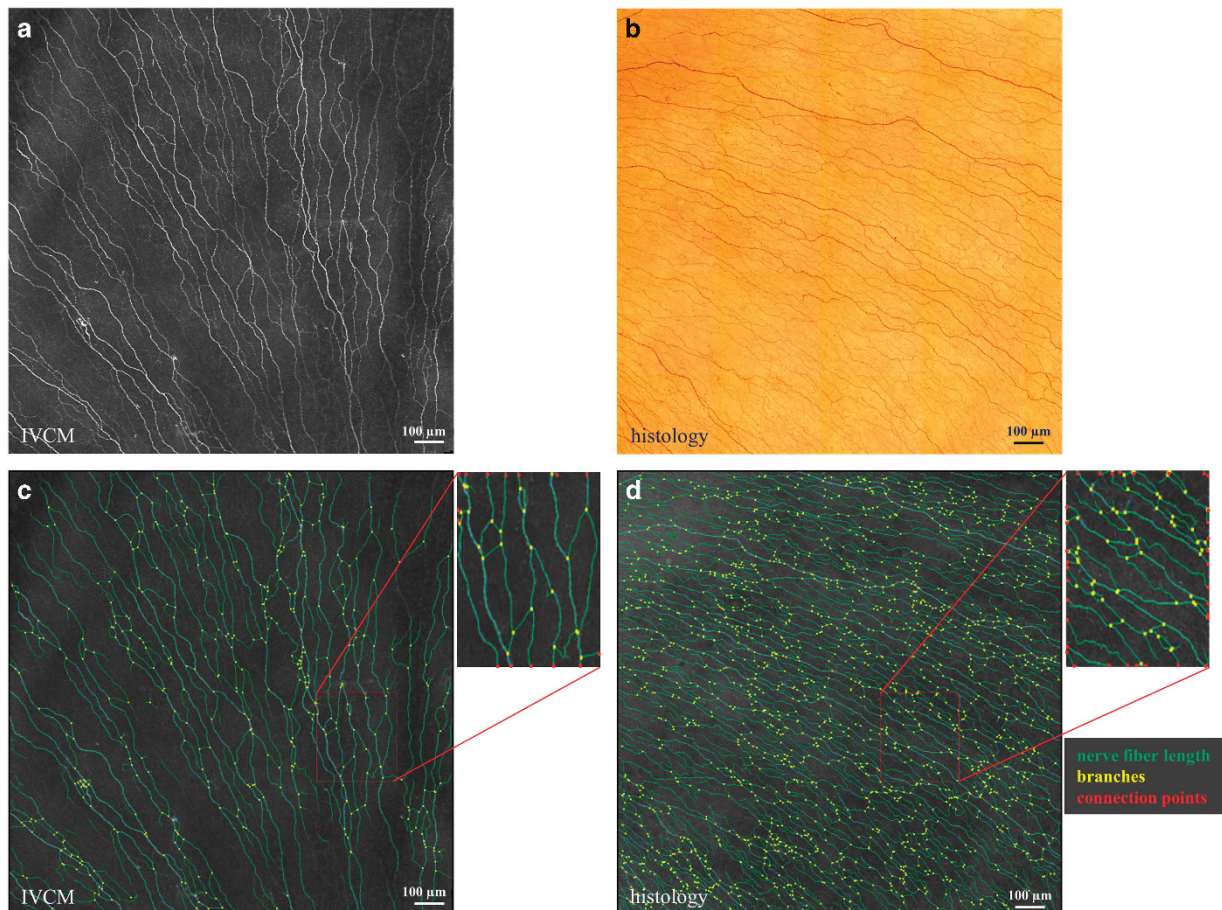


Figure 1 SBP in images from IVCM and histology. (a) IVCM mosaic image of the human corneal SBP depicting corneal nerve fibers; (b) histological staining of the human corneal SBP showing β -III- tubulin-stained corneal nerves; and (c and d) represent the results of segmentation from the corresponding SBP images, respectively. Scale bar, 100 μ m.

Table 1 Properties of the analyzed images

(A)	Subject age (years)	Mean ± SD	P-value
IVCM	44	37.25 ± 8.3	0.029
	26		
	36		
	43		
Histology	49	61.2 ± 18.1	
	61		
	87		
	48		
(B)	Image area (mm ²)	Mean ± SD	P-value
IVCM	2.419	2.425 ± 0.004	0.343
	2.427		
	2.425		
	2.427		
Histology	2.543	2.576 ± 0.263	
	2.256		
	2.898		
	2.605		

analyzed images and their properties are presented in Figure 1 and Table 1.

A large number of pixels within the four image areas were identified as center points of hypothetical IVCM image frames. All these valid hypothetical frames were extracted and submitted to image analysis individually in order to derive local values for all SNP parameters. A set of parameters for each image section including CNFL, CNFD, CNBD, CNFTo, CNCP, CNSFL, and CNFTh was calculated and compared. Reference values for the whole reconstructed image areas as well as descriptives for all valid frames of the four IVCM and four histology images are presented in Table 2.

The measured values of the four histology images for the parameters CNFL, CNFD, CNBD, CNFTo, and CNCP manifested a clear increase compared with the corresponding four IVCM mosaic images. In contrast, the corresponding CNSFL values showed a clear increase in IVCM images. Even though there was variation in nerve fiber thickness between IVCM and histology images, there was no difference observed in the values for the parameter CNFTh after quantification (Table 2).

Computed heat maps for CNFL (Figure 2a) show comparable inhomogeneous SBP networks in IVCM and IHC images. Distinct accumulations of nerve fiber bundles (hot spots) and greater areas with low local values can be observed. Density plots provide unique insight into the distribution and high-value range of local parameter values and further indicate SBP inhomogeneity (Figure 2b). Mean values of all single frames (green marker) differ slightly from the value of the reference

image (red marker) in the IVCM image, while this difference is even smaller for the presented IHC image.

Discussion

IVCM has been used with increasing frequency in recent years to provide high contrast *in vivo* visualization of the corneal SBP in health and disease;²³ however, the ability of this method to quantify optimally all morphological parameters of the corneal SBP remains uncertain.² In this regard, it is essential to study and understand if there exists any systematic assessment differences during image quantification by comparison of IVCM obtained SBP images with *ex vivo* images of SBP taken from histological sections. Since immunohistochemistry quantification is also employed in clinical practice,¹⁵ the comparisons of IVCM quantification data with histology will presumably assist and also likely represent the true values of intact SBP.

During the quantification of IVCM and histology images, an area of the central corneal SBP ~2 mm away from the whorl region was chosen in order to make the images comparable. We adopted the pixel size to be nearly the same in IVCM and histology (IVCM images pixel size: 1.08 μm²; histology images were captured at × 20 with a pixel size of 0.24 μm² and exported at × 5 with a pixel size of 0.97 μm²) and used them for quantification.

Quantitative assessment of CNFL is regarded as the single most reliable parameter of SBP structural and functional integrity.²⁴ In the present study, using our quantification software, the mean CNFL value in the IVCM images (21.7 mm/mm² ± 2.1) was comparable to CNFL baseline values reported previously (19.00 mm/mm² ± 4–5; 22.20–23.63 mm/mm²).^{4,24} Similarly, the measured mean CNFL value of histology images (50.0 mm/mm² ± 3.9) matches values (45.94 mm/mm² ± 5.2) reported previously.¹⁷ The median CNFL values calculated in this study by histology is approximately two times greater than previous high estimates (21.6 ± 5.98 and 25.9 ± 7.0 mm/mm²) based on IVCM observations.^{25,26} One explanation for these higher values seen by histology is that the immunochemical staining method dependably detects small diameter sub-basal nerves and interconnecting axons that are too thin or faint to be imaged reliably by IVCM.²⁴

IVCM, with a limited lateral resolution of 1–2 μm,²⁷ enables enface imaging of the SBP and its nerve fiber bundles. In contrast, the β-III-tubulin immunohistochemical staining method, by exploiting the phenomenon of histochemical amplification of the avidin-biotin-horseradish peroxidase complex methodology and a strong ‘signal to noise’ ratio, is able to detect more minute patterns of corneal SBP anatomy including

very small diameter nerve fiber bundles, interconnecting single nerve fiber branches and their connection points (Figure 3).

Therefore, in our study, it is not surprising to observe higher CNSFL values in the images from IVCM compared with histology (Table 2). Likewise, this same reason also

Table 2 Measures of the various SBP parameters

Parameter	Image	Reference value	Median (IQR)	P-value
CNFL nerve fiber length (mm/mm ²)	IVCM	19.9 19.9 24.0 23.0	21.4 (3.3)	0.020
	Histology	47.5 53.9 45.8 52.9	50.2 (6.0)	
CNFD nerve fiber density (<i>n</i> per mm ²)	IVCM	254.7 187.5 299.8 334.2	277.3 (70.5)	0.021
	Histology	1442.0 1275.6 1091.0 1672.1	1358.8 (270.1)	
CNBD number of branching points (<i>n</i> per mm ²)	IVCM	146.4 95.6 180.6 193.3	163.5 (50.1)	0.021
	Histology	914.3 780.9 678.7 1064.5	847.6 (196.5)	
CNFTo average weighted tortuosity (μm^{-1})	IVCM	0.0788 0.0830 0.0813 0.0820	0.081 (0.001)	0.021
	Histology	0.1006 0.0860 0.0910 0.0990	0.095 (0.009)	
CNCP Number of connecting points (<i>n</i> per mm ²)	IVCM	20.6 22.2 21.0 31.3	21.6 (3.5)	0.021
	Histology	49.9 54.9 48.9 47.2	49.4 (2.6)	
CNSFL average single-fiber length (μm)	IVCM	73.1 101.8 75.1 63.8	74.1 (10.9)	0.021
	Histology	27.6 37.0 36.7 26.3	32.18 (9.55)	
CNFTh average weighted nerve fiber thickness (μm)	IVCM	2.244 2.203 2.198 2.302	2.224 (0.057)	0.309
	Histology	2.225 2.157 2.207 2.198	2.202 (0.024)	

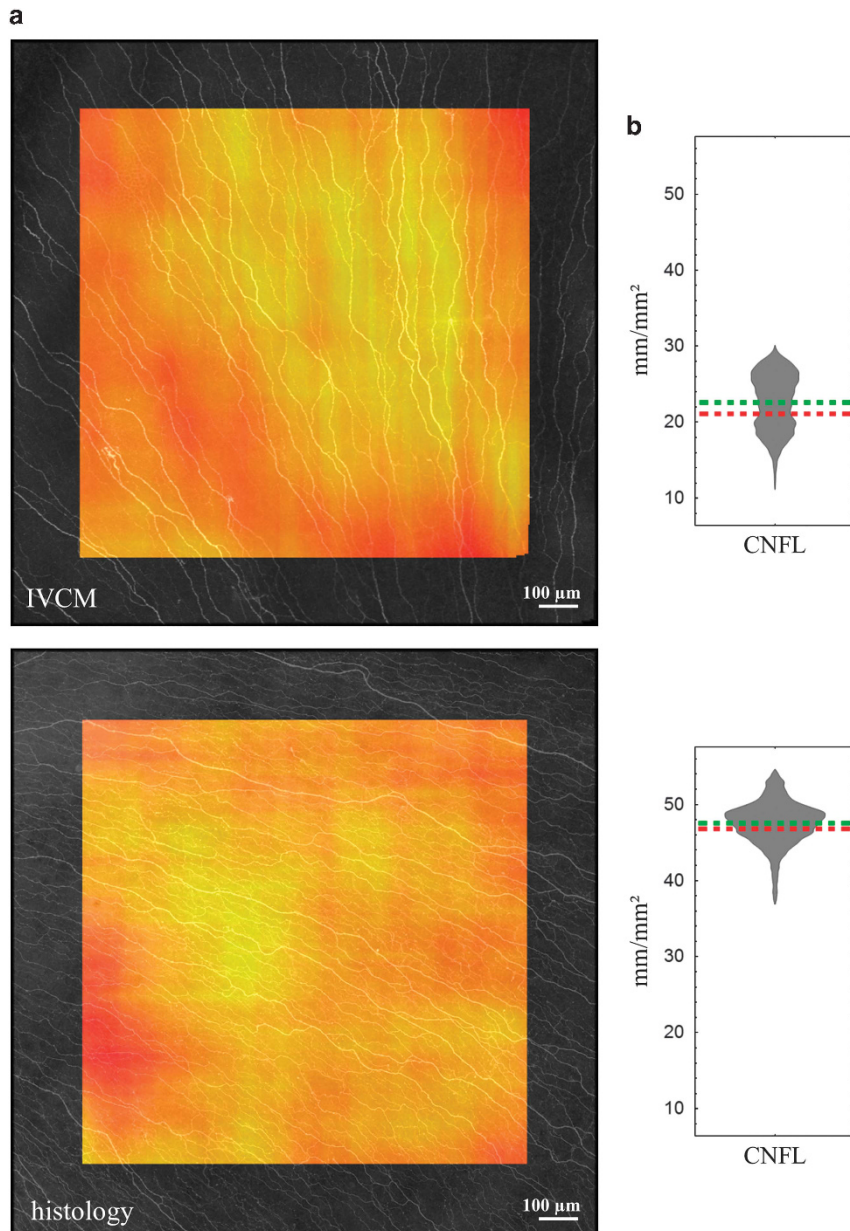


Figure 2 Local variability of the parameter CNFL. CNFL parameter local variability was calculated using published and dedicated algorithms. Heat maps (a) and density plots (b) of CNFL parameter values (in IVCM and histology images, respectively) for frames at all center positions showing local variations based on nerve fiber distribution and local fiber properties. The red lines in the plots indicate the reference value calculated for the total image areas whereas the green lines indicate the mean value of all single frames. Considerable difference in the reference and mean values was observed in IVCM mosaicking image whereas no such difference between reference and mean values for the parameter CNFL was observed in histology. Scale bar, 100 μm .

explains the higher CNFD and CNBD values in histology images than in IVCM images (Table 2). Since the corneal nerve branching pattern is unequivocally visualized in histology images, one can predict a greater number of corneal nerve connection points in histology images than in IVCM images (Table 2). The results of the current study also revealed a small increase in CNFTo in histology

images. Even though the observed difference in our study is in line with the recent report of age-dependent increase in tortuosity,⁴ the small sample size examined in our study and the relatively small difference in mean age between the histology and IVCM groups, prevented us from drawing any meaningful conclusions on age-related changes in SBP tortuosity. Furthermore, no clear

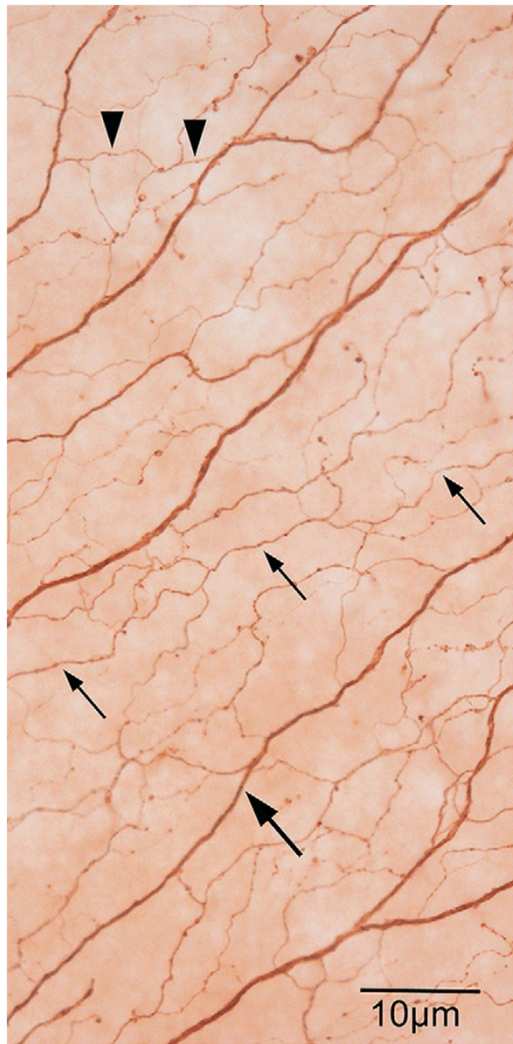


Figure 3 Example of healthy human corneal sub-basal nerve plexus. Large arrow indicates a thick sub-basal nerve fiber; small arrows indicate thin sub-basal nerve fibers; and arrowheads indicate interconnecting fibers. Scale bar, 10 μm . Reproduced with permission from Marfurt *et al.*¹⁷

difference in CNFTh was observed in our comparison study between IVCM and histology images. This was mainly attributable to the post-processing and it is possible that this is an image artifact caused in part by the employed segmentation procedure which produces a slight over-segmentation of nerve fiber structures in order to increase detection rate.

Because single IVCM images ($400 \times 400 \mu\text{m}^2$) demonstrate only a small fraction ($<0.2\%$) of the total corneal surface,¹⁰ IVCM imaging and quantification of the corneal SBP on the basis of a small number of such single images may be strongly affected by local SBP variation.⁵ In the present study, we compared local variations of the CNFL parameter in IVCM and histological images by

using heat maps. Heat maps are an appropriate tool for the visualization of inhomogeneously distributed elements of the SBP. The respective density plots express high-value ranges of CNFL and thus give evidence of parameter variability. Furthermore they illustrate varied actual parameter value distribution for the parameter CNFL between IVCM and histology images, which cannot be achieved by using standard box plots.

Another limitation of the current study is that the corneas selected for quantification are from different age groups (mean age: IVCM = 37.25 ± 8.3 ; histology = 61.25 ± 18.1). It is known that CNFL decreases slightly with age (0.25–0.3% (ref. 24) or $0.05 \text{ mm}/\text{mm}^2$ (ref. 28) per year), and incorporating this variable into our interpretation would adjust the CNFL of the *ex vivo* corneas by $1.2 \text{ mm}/\text{mm}^2$ ($48.8 \text{ mm}/\text{mm}^2$). This will not influence our quantification results because aging does not essentially affect the density of the SBP in the human central cornea.^{17,29} IVCM with its merit of non-invasive *in vivo* observation of SBP architecture without prior staining could serve as a powerful and valuable diagnostic tool for the analysis of corneal nerve morphology during health and disease. The observed differences in many SBP quantitative measurements between these two methodologies are explained by the higher resolution of the histology images compared with IVCM images.

In conclusion, IVCM is an invaluable method for non-invasive visualization of the human corneal SBP clinically; however, inherent limitations in IVCM image resolution, compared with *ex vivo* histological staining, result in an appreciable underestimation of several SBP parameters. This limitation should always be considered during its usage in clinical practice. Furthermore, this study also compared the SBP local variability of IVCM with histology. Since it is known that significant proportion of the SBP may be missed with IVCM because of its methodological limitations and histology could be able to demonstrate intraepithelial nerve terminals,³⁰ we hypothesized that images acquired by histology method show complete, unaltered SBP networks with less difference in local variability than images from IVCM. This could imply potential clinical relevance because parameters can be calculated more reliably from fully demonstrated, undistorted SBP networks. Our results may have clinical significance since evaluation of the SBP parameters is indispensable in the clinical usage of IVCM.

Technical considerations

It cannot be ruled out that some postmortem tissue shrinkage occurs during excision and fixation of donor corneas, and that this phenomenon may influence SBP density calculations.³¹ Although recognizing this

possibility, it seems unlikely that the human cornea, consisting of ~200 layers of densely packed inflexible collagenous fibers, is susceptible to significant postmortem contraction. The rigid corneal stroma, in turn, would provide a stable backbone on which the overlying corneal epithelium and its constituent SBP would be 'protected' from significant shrinkage. Freezing, immunohistochemical staining, and air-drying of the corneal specimens onto glass slides did not contribute to specimen shrinkage in our study. The mean 'starting diameters' of the formalin-fixed corneal buttons were essentially unchanged when measured later, using a calibration bar in a light microscope, after they were mounted and coverslipped on glass slides (data not shown). In the mammalian cornea, the SBP is essentially a two-dimensional structure and has minimal 'depth'. During imaging of the IHC specimens, sub-basal nerve fibers that lie 'above' or 'below' the plane of focus were not missed since the entire SBP nerve fibers lie within the same, relatively thin plane.

Summary

What was known before

- Confocal microscopy of the corneal sub-basal nerve plexuses.
- Histology of the corneal sub-basal nerve plexes.

What this study adds

- In this study, we compared the human corneal sub-basal nerve plexus images obtained by *in vitro* confocal microscopy and histology to compare and contrast quantitative data of the human corneal sub-basal nerve plexus.

Conflict of interest

The authors declare no conflict of interest.

Acknowledgements

This work was supported in part by DFG (KO-4979/1-1) and BMBF (RESPONSE).

References

- 1 Tavakoli M, Quattrini C, Abbott C, Kallinikos P, Marshall A, Finnigan J *et al.* Corneal confocal microscopy: a novel noninvasive test to diagnose and stratify the severity of human diabetic neuropathy. *Diabetes Care* 2010; **33**(8): 1792–1797.
- 2 Shtein RM, Callaghan BC. Corneal confocal microscopy as a measure of diabetic neuropathy. *Diabetes* 2013; **62**(1): 25–26.
- 3 Ziegler D, Papanas N, Zhivov A, Allgeier S, Winter K, Ziegler I *et al.* Early detection of nerve fiber loss by corneal confocal microscopy and skin biopsy in recently diagnosed type 2 diabetes. *Diabetes* 2014; **63**: 2454–2463.
- 4 Tavakoli M, Ferdousi M, Petropoulos IN, Morris J, Pritchard N, Zhivov A *et al.* Normative values for corneal nerve morphology assessed using corneal confocal microscopy: a multinational normative data set. *Diabetes Care* 2015; **38**(5): 838–843.
- 5 Winter K, Scheibe P, Köhler B, Allgeier S, Guthoff RF, Stachs O. Local variability of parameters for characterization of the corneal subbasal nerve plexus. *Curr Eye Res* 2016; **41**(2): 186–198.
- 6 Turuwheua JT, Patel DV, McGhee CN. Fully automated montaging of laser scanning *in vivo* confocal microscopy images of the human corneal subbasal nerve plexus. *Invest Ophthalmol Vis Sci* 2012; **53**(4): 2235–2242.
- 7 Edwards K, Pritchard N, Gosschalk K, Sampson GP, Russell A, Malik RA *et al.* Wide-field assessment of the human corneal subbasal nerve plexus in diabetic neuropathy using a novel mapping technique. *Cornea* 2012; **31**(9): 1078–1082.
- 8 Allgeier S, Maier S, Mikut R, Peschel S, Reichert KM, Stachs O *et al.* Mosaicking the subbasal nerve plexus by guided eye movements. *Invest Ophthalmol Vis Sci* 2014; **55**(9): 6082–6089.
- 9 Zhivov A, Winter K, Hovakimyan M, Peschel S, Harder V, Schober HC *et al.* Imaging and quantification of subbasal nerve plexus in healthy volunteers and diabetic patients with or without retinopathy. *PLoS One* 2013; **8**(1): e52157.
- 10 Winter K, Allgeier S, Eberle F, Köhler B, Maier S, Stachs O *et al.* Software-based imaging and segmentation of corneal nerve fibres. *Biomed Tech (Berl)* 2013; **58**(suppl 1): doi:10.1515/bmt-2013-4293.
- 11 Petropoulos IN, Alam U, Fadavi H, Marshall A, Asghar O, Dabbah MA *et al.* Rapid automated diagnosis of diabetic peripheral neuropathy with *in vivo* corneal confocal microscopy. *Invest Ophthalmol Vis Sci* 2014; **55**(4): 2071–2078.
- 12 Dehghani C, Pritchard N, Edwards K, Russell AW, Malik RA, Efron N. Fully automated, semiautomated, and manual morphometric analysis of corneal subbasal nerve plexus in individuals with and without diabetes. *Cornea* 2014; **33**(7): 696–702.
- 13 Sindt CW, Lay B, Bouchard H, Kern JR. Rapid image evaluation system for corneal *in vivo* confocal microscopy. *Cornea* 2013; **32**(4): 460–465.
- 14 Coleman R. The impact of histochemistry—a historical perspective. *Acta Histochem* 2000; **102**(1): 5–14.
- 15 Matos LL, Trufelli DC, de Matos MG, da Silva Pinhal MA. Immunohistochemistry as an important tool in biomarkers detection and clinical practice. *Biomark Insights* 2010; **5**: 9–20.
- 16 Teruya-Feldstein J. The immunohistochemistry laboratory: looking at molecules and preparing for tomorrow. *Arch Pathol Lab Med* 2010; **134**(11): 1659–1665.
- 17 Marfurt CF, Cox J, Deek S, Dvorscak L. Anatomy of the human corneal innervation. *Exp Eye Res* 2010; **90**(4): 478–492.
- 18 Al-Aqaba MA, Fares U, Suleman H, Lowe J, Dua HS. Architecture and distribution of human corneal nerves. *Br J Ophthalmol* 2010; **94**(6): 784–789.
- 19 He J, Bazan NG, Bazan HE. Mapping the entire human corneal nerve architecture. *Exp Eye Res* 2010; **91**(4): 513–523.
- 20 Kheirkhah A, Muller R, Mikolajczak J, Ren A, Kadas EM, Zimmermann H *et al.* Comparison of standard versus wide-field composite images of the corneal subbasal layer by *in vivo* confocal microscopy. *Invest Ophthalmol Vis Sci* 2015; **56**(10): 5801–5807.
- 21 Köhler B, Allgeier S, Stachs O, Winter K, Bretthauer G. Software-based imaging and quantitative analysis of the

- corneal sub-basal nerve plexus. *Nova Acta Leopold* 2014; **119**(401): 127–142.
- 22 Allgeier S, Zhivov A, Eberle F, Köhler B, Maier S, Bretthauer G *et al*. Image reconstruction of the subbasal nerve plexus with *in vivo* confocal microscopy. *Invest Ophthalmol Vis Sci* 2011; **52**: 5022–5028.
- 23 Jiang MS, Yuan Y, Gu ZX, Zhuang SL. Corneal confocal microscopy for assessment of diabetic peripheral neuropathy: a meta-analysis. *Br J Ophthalmol* 2015; **100**: 9–14.
- 24 Parissi M, Karanis G, Randjelovic S, Germundsson J, Poletti E, Ruggeri A *et al*. Standardized baseline human corneal subbasal nerve density for clinical investigations with laser-scanning *in vivo* confocal microscopy. *Invest Ophthalmol Vis Sci* 2013; **54**(10): 7091–7102.
- 25 Niederer RL, Perumal D, Sherwin T, McGhee CN. Corneal innervation and cellular changes after corneal transplantation: an *in vivo* confocal microscopy study. *Invest Ophthalmol Vis Sci* 2007; **48**(2): 621–626.
- 26 Patel DV, Ku JY, Johnson R, McGhee CN. Laser scanning *in vivo* confocal microscopy and quantitative aesthesiometry reveal decreased corneal innervation and sensation in keratoconus. *Eye (Lond)* 2009; **23**(3): 586–592.
- 27 Jalbert I, Stapleton F, Papas E, Sweeney DF, Coroneo M. *In vivo* confocal microscopy of the human cornea. *Br J Ophthalmol* 2003; **87**(2): 225–236.
- 28 Dehghani C, Pritchard N, Edwards K, Vagenas D, Russell AW, Malik RA *et al*. Morphometric stability of the corneal subbasal nerve plexus in healthy individuals: a 3-year longitudinal study using corneal confocal microscopy. *Invest Ophthalmol Vis Sci* 2014; **55**(5): 3195–3199.
- 29 Erie JC, McLaren JW, Hodge DO, Bourne WM. The effect of age on the corneal subbasal nerve plexus. *Cornea* 2005; **24**(6): 705–709.
- 30 Tervo T, Holopainen J, Belmonte C. Confocal microscopy of corneal nerves—a limited but still useful technique to evaluate peripheral neuropathies. *JAMA Ophthalmol* 2016; **134**(9): 990–991.
- 31 Müller LJ, Marfurt CF, Kruse F, Tervo TM. Corneal nerves: structure, contents and function. *Exp Eye Res* 2003; **76**(5): 521–542.